Vapor-liquid equilibria for binary systems carbon dioxide + 1,1,1,2,3,3-hexafluoro-3-(2,2,2-trifluoroethoxy)propane or 1-ethoxy-1,1,2,2,3,3,4,4,4-nonafluorobutane at 303.15–323.15 K

Hiroyuki Matsuda [a,*], Toru Suga [a], Tomoya Tsuji [b], Katsumi Tochigi [a], Kiyofumi Kurihara [a], Alyssa K. Nelson [c,d], Clare McCabe [c,d,e]

[a] Department of Materials and Applied Chemistry, Nihon University, 1-8-14 Kanda Surugadai, Chiyoda-ku, Tokyo 101-8308, Japan
[b] Department of Chemical Process Engineering, Universiti Teknologi Malaysia Kuala Lumpur, Off Jalan Sultan Yahya Petra 54100, Kuala Lumpur, Malaysia
[c] Department of Chemical and Biomolecular Engineering, Vanderbilt University, Nashville, TN, 37212, United States
[d] Multiscale Modeling and Simulation Center, Vanderbilt University, Nashville, TN, 37212, United States
[e] Department of Chemistry, Vanderbilt University, Nashville, TN 37212, United States

ARTICLE INFO

ABSTRACT

The phase behavior of binary mixtures of carbon dioxide (CO_2) and hydrofluoroethers (HFEs) has been studied. In particular, experimental vapor-liquid equilibrium (VLE) data for CO_2 + 1,1,1,2,3,3-hexafluoro-3-(2,2,2-trifluoroethoxy)propane (HFE-449mec-f) and 1-ethoxy-1,1,2,2,3,3,4,4,4-nonafluorobutane (HFE-7200) at temperatures of 303.15, 313.15, and 323.15 K are reported. The VLE data were measured using a static-type apparatus and then correlated using the Peng-Robinson equation of state with the van der Waals one fluid and Wong-Sandler-NRTL mixing rules. Reasonable correlation results were obtained from the Peng-Robinson equation of state with both the van der Waals one fluid and the Wong-Sandler-NRTL mixing rules. The GC-SAFT-VR equation also gave good predictions of the phase behavior. Additionally, the group contribution SAFT-VR (GC-SAFT-VR) equation was used to predict the experimental VLE in good agreement with the experimental data, as well as the full *p,T* phase diagram for both systems.

© 2020 Elsevier B.V. All rights reserved.

1. Introduction

Chlorofluorocarbons (CFCs) have been utilized extensively as refrigerants, blowing agents, and cleaning solvents due to their chemical stability and physical properties. However, the Montreal Protocol (1989) requested that the use of CFCs be phased-out prior to 1996 because of ozone layer depletion and global warming. Thus, CFC alternatives have been investigated heavily in subsequent years. Hydrochlorofluorocarbons (HCFCs) have been used as interim replacements for CFCs because of similar physicochemical properties and lower ozone depletion potential (ODP) values; however, it should be noted that they have higher global warming potential (GWP) values. Thus, they are to be phased-out by 2020 according to the updated Montreal Protocol. Hydrofluorocarbons (HFCs) and perfluorocarbons (PFCs) have been used as alternatives to CFCs and HCFCs, because they have zero ODP and high thermal stabilities; however, they still have high GWP values. There-fore, HFCs and PFCs were included in the set of six major greenhouse gasses whose use should be reduced in the Kyoto Protocol (2005). As a result, hydrofluoroethers (HFEs) have been utilized as third generation alternatives to replace CFCs, HCFCs, HFCs, and PFCs due to their zero ODP, low GWP, and short atmospheric lifetimes [1–5]. Industrially HFEs are also used as cleaning solvents in electronic and magnetic devices, as a protective gas in the melting of alloys, for decontamination of fluids, and as heat transfer fluids in heat exchangers [6,7]. However, pure HFE's are flammable and toxic. Thus, a mixture of HFE's with another refrigerant could retain desirable properties, whilst negating some of the more undesirable ones, and has been a successful strategy in the past (e.g., hydrofluoroolefins [8,9]).

Carbon dioxide (CO_2) is a well-known natural refrigerant that can be used as an alternative to the above-mentioned CFCs, HCFCs, HFCs, and PFCs, making it a possible refrigerant to use in mixtures with HFE's. CO_2 is a natural, nontoxic, readily available and inflammable gas with zero ODP. Because of these favorable physical properties, CO_2 has already been used as a working fluid for heat pumps [10]. However, one of the main disadvantages is that

List of symbols

a	energy parameter in the PR EOS (Pa m^6 mol^{-2})
A	Helmholtz free energy (J mol^{-1})
b	size parameter in the PR EOS (m^3 mol^{-1})
C	constant in the WS model
A, B, C	Antoine constants
F_{obj}	objective function
$g_{ij} - g_{jj}$	binary interaction parameter in the NRTL model (J mol^{-1})
k_{12}	second virial coefficient binary interaction parameter in the WS model
k_{12}	binary interaction parameter in the PR EOS
l_{12}	binary interaction parameter in the PR EOS
m_i	parameter in the PR EOS
NC	number of pure components in the system
NDP	number of data points per system
P	pressure (Pa)
P^s	saturated vapor pressure (kPa)
$|\Delta P/P|$	relative deviation between experimental and calculated equilibrium pressures
R	gas constant (8.314 J mol^{-1} K^{-1})
r	distance between the two groups
T	absolute temperature (K)
v	molar volume (m^3 mol^{-1})
x	liquid phase mole fraction
y	vapor phase mole fraction
$|\Delta y_1|$	absolute deviation between experimental and calculated vapor phase mole fractions of component 1

Greek letters

α_{12}	non-randomness parameter in the NRTL model
ω	acentric factor
ρ	density (kg m^{-3})

Superscript

E	excess property
ideal	ideal
s	saturated

Subscripts

1, 2, i, j, k	components 1, 2, i, j, and k
∞	infinite pressure condition
av.	average
c	critical
calcd.	calculated
exptl.	experimental
r	reduced

Fig. 1. Structures of HFE-449mec-f and HFE-7200.

CO_2 run heat pumps need to be operated in a trans-critical cycle, i.e., at a very high pressure (typically within 15 MPa of the maximum operating pressure), due to its relatively low critical constants (T_c = 304.12 K, P_c = 7.374 MPa [11]) [12,13]. Mixtures of CO_2 and HFEs may thus also provide a promising alternative by reducing the need for a high operating pressure whilst retaining the more favorable properties of CO_2.

In order to evaluate the performance of mixtures of CO_2 and HFEs and determine optimal operating conditions for refrigeration processes using mixtures of CO_2 and HFEs, an understanding of the mixture vapor-liquid equilibrium (VLE) data is crucial. Several studies report experimental VLE data for binary mixtures of CO_2 + CFCs [13–22]. However, limited VLE data is available in the literature regarding binary systems CO_2 + HFEs. The object of this work is thus to measure the VLE data for binary systems CO_2 + HFEs, i.e., 1,1,1,2,3,3-hexafluoro-3-(2,2,2-trifluoroethoxy)propane (HFE-449mec-f) and 1-ethoxy-
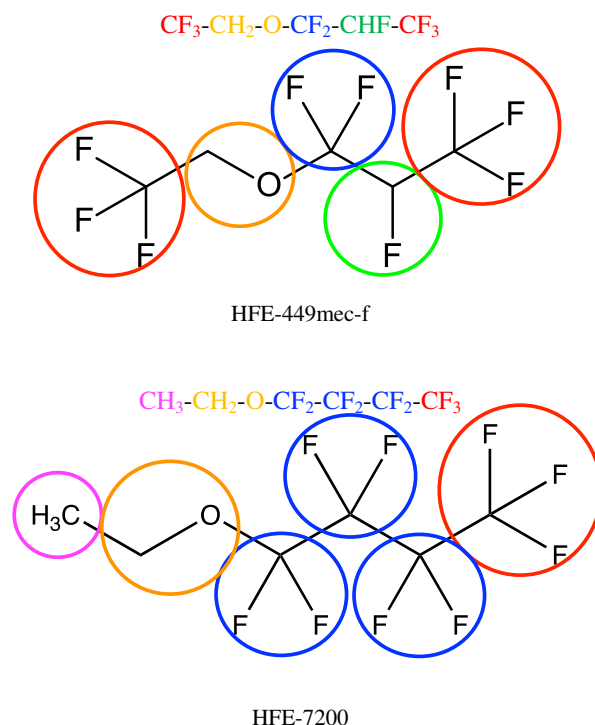
1,1,2,2,3,3,4,4,4-nonafluorobutane (HFE-7200). The structures of the two HFEs studied are shown in Fig. 1. These two HFEs were chosen because HFE-449mec-f can also be used as an alternative cleaning solvent [2,22,23] and HFE-7200 has lower values of GWP and atmospheric lifetime compared to other HFEs (60 and 0.77 years, respectively [1]). It can be used not only as a working fluid for refrigerants and heat transfer, but also as a cleaning solvent and lubricant carrier, etc. [7,24]. We determined the isothermal VLE for CO_2 + HFE-449mec-f or HFE-7200 at temperatures 303.15, 313.15, and 323.15 K using a static-circulation apparatus. The experimental VLE data were correlated by the Peng-Robinson (PR) equation of state (EOS) [25] coupled with the van der Waals one fluid (vdW1) mixing rule and Wong-Sandler (WS) [26] mixing rules combined with the non-random two-liquid (NRTL) model [27]. The systematic series of experimental data are also described with the group contribution (GC) based SAFT-VR [28] equation of state (GC-SAFT-VR) that combines the SAFT-VR [29] equation with a group contribution [28] approach. The GC-SAFT-VR equation describes chains composed of neutral non-polar square-well spheres of different sizes and/or interaction energies (including dispersion and association), with monomer properties computed from perturbation theory using a reference system of hard spheres of arbitrary composition and size. Using this hetero-segmented approach, GC-SAFT-VR parameters have been determined in prior work for a wide range of functional groups (i.e., CH$_3$, CH$_2$, C=O, CH$_2$O, OH, etc.) and used to study the thermodynamics and phase behavior of alkanes, alkenes, ketones, aromatics, acetates, esters, polymers, and other associating and non-associating fluids (see for example [5,28,30–32]). We note that the cross interactions between simple groups such as CH$_3$-CH$_2$ are given by the simple Lorentz-Berthelot combining rules; however, for cross interactions with polar groups, such as the carbonyl group, where deviations from "ideal behavior" are expected, the cross interactions are fitted to pure component experimental data for molecules that contain the functional groups under consideration. In this way, in contrast to the traditional equation of state and SAFT-based approaches, when devia-

Table 1
Chemicals used in this work.

Component	Source	CAS Registry Number	Purification method	Purity	ρ (298.15 K) (kg m^{-3}) Experimental [f]	Literature
CO_2	Showa Denko Gas Products Co. Ltd.	124-38-9	No	0.9999 [d]	–	–
HFE-449mec-f [a]	DAIKIN Fine Chemical Co. Ltd.	993-95-3	Molecular sieves 13X	0.995 [e]	1527.97	1531.2 [g]
HFE-7200 [b]	3M Co. Ltd.	163702-06-5 [c] 163702-05-4 [c]	Molecular sieves 5A	0.999 [e]	1422.56	1422.65 [h]

[a] IUPAC name: 1,1,1,2,3,3-hexafluoro-3-(2,2,2-trifluoroethoxy)propane.
[b] IUPAC name: 1-ethoxy-1,1,2,2,3,3,4,4,4-nonafluorobutane.
[c] Binary mixture of two isomers with mole fraction of 0.614 for CAS number 163702-06-5 and 0.386 for CAS 163702-05-4, determined by ^{1}H NMR, with a standard uncertainty $u(x) = 0.01$.
[d] volume fraction.
[e] mass fraction.
[f] At $P = 101$ kPa. Standard uncertainties are $u(\rho) = 0.01$ kg m^{-3}, $u(T) = 0.01$ K, and $u(P) = 1$ kPa.
[g] Tochigi et al. [42]. At $T = 293.15$ K.
[h] Rausch et al. [7].

tions from the Lorentz-Berthelot combining rule are seen, parameters do not need to be fit to experimental mixture data. Additionally, by not averaging the group parameters on chain formation, as in other group-contribution based SAFT approaches [33–35], the connectivity of functional groups and location of association sites can be specified in the GC-SAFT-VR approach.

Multiple SAFT approaches have been proven effective in the study of a wide variety of refrigerants, including fluorinated systems, such as the SAFT-VR study by Galindo et al. [36] and the work of Avendaño et al. [37] who studied pure refrigerants with the SAFT-gamma group-contribution approach. Additionally, fluorinated refrigerant mixtures have also been studied using GC-SAFT-VR and PC-SAFT in work by Haley et al. [5] and Fouad and Vega [9], respectively. In this work, we expand upon previous work with the GC-SAFT-VR approach in order to predict the phase behavior of the CO_2 + HFE binary mixtures studied and provide a wider examination of their phase behavior than is possible with correlative approaches.

2. Experimental section

2.1. Materials

The chemicals used in this work are summarized in Table 1. The CO_2 was passed through a 0.5 μm inline filter (Nepro Company, Japan) before use to avoid undesirable particles. The purity of the HFE-449mec-f and HFE-7200 was verified by gas chromatography (GC) (GC-14A, Shimadzu Co. Ltd., Kyoto, Japan) with a thermal conductivity detector. Existence of two isomers has been reported in the literature [7,38–41]. Thus, the composition of binary isomers of HFE-7200 was determined by ^{1}H NMR analysis (JNM-ECX400, JEOL Ltd., Tokyo, Japan). The obtained mole fraction of the isomer with CAS number 163702-06-5 was 0.614, whereas that of the isomer with CAS 163702-05-4 was 0.386. The densities (ρ) of the esters at 298.15 K was measured using a precision digital oscillating U-tube densimeter (DMA 4500, Anton Paar GmbH, Graz, Austria) with a reproducibility of 10^{-2} kg m^{-3}. The experimental ρ at 298.15 K for the chemicals used in this work are reported in Table 1 together with the literature values [7,42].

2.2. Apparatus and procedure

We used a static-circulation apparatus to measure the VLE. A schematic diagram of the apparatus is shown in Fig. 2. It is composed of three parts, i.e., a variable volume equilibrium cell, sampling unit for vapor and liquid phases, and GC. The equilibrium cell 1 was immersed in a thermostated water bath with three windows (THOMAS KAGAKU Co. Ltd., Japan). There are six visual sapphire windows (23 mm in diameter and 11.5 mm thick) in the equilibrium cell for the visual observation of the phase behavior.

The temperature of the apparatus was controlled within ± 0.1 K. The equilibrium cell was made from stainless steel (SUS 316) and measurements can be made at temperatures up to 473 K and pressures up to 20 MPa. The inner volume was 500 cm^3. A calibrated Pt 100 Ω platinum resistance thermometer 4 with an accuracy of ± 0.01 K was used for measurements of the sample temperature. The pressure was determined by a pressure indicator (DPI 145, Druck Co., Kirchentellinsfurt, Germany) with an accuracy of ± 0.04% F.S. Two GCs were used for the analysis of the vapor and liquid phase samples, respectively. Further details regarding the experimental apparatus and procedure have been described in previous work [21].

During measurement, first, the equilibrium cell (labelled 1 in Fig. 2) was evacuated by the vacuum pump, and HFE-449mec-f or HFE-7200 was charged into the equilibrium cell. Next, CO_2 was added until the desired pressure is achieved. Then, the liquid phase was continuously recirculated (through circulation 14 in Fig. 2). The interface of the vapor and liquid phases were observed during the measurements by the visual glass windows equipped in the cell. The system was regarded as reaching equilibrium when temperature and pressure fluctuations of no more than ±0.01 K and ±0.001 MPa, respectively, were observed for 30 min. The equilibrium measurement of temperature and pressure before sampling was up to about 6 hours.

Once equilibrium was reached, the vapor and liquid samples were taken (Sample injector 15 in Fig. 2). Finally, the compositions of the vapor and liquid phases were determined by GC.

2.3. Analysis

The vapor and liquid phase samples were analyzed by a GC (GC-14A, Shimadzu Co., Ltd., Kyoto, Japan) with a thermal conductivity detector (TCD). Porapak Q (2.0 m × 3.0 mm inside diameter, Shinwa Chemical Industries Ltd., Kyoto, Japan) was used as the column packing. Helium was used as the carrier gas at a flow rate of 50.0 mL min^{-1}. The temperature in the TCD was maintained at 623 K. Compositions were determined using the absolute area method with a calibration curve. The accuracy for the mole fraction was ± 0.002.

3. Models and theory

3.1. Peng-Robinson equation of state

The correlations of the experimental VLE data were performed with the PR EOS combined with the vdW1 or WS-NRTL models as the mixing rule. The PR EOS is given by,

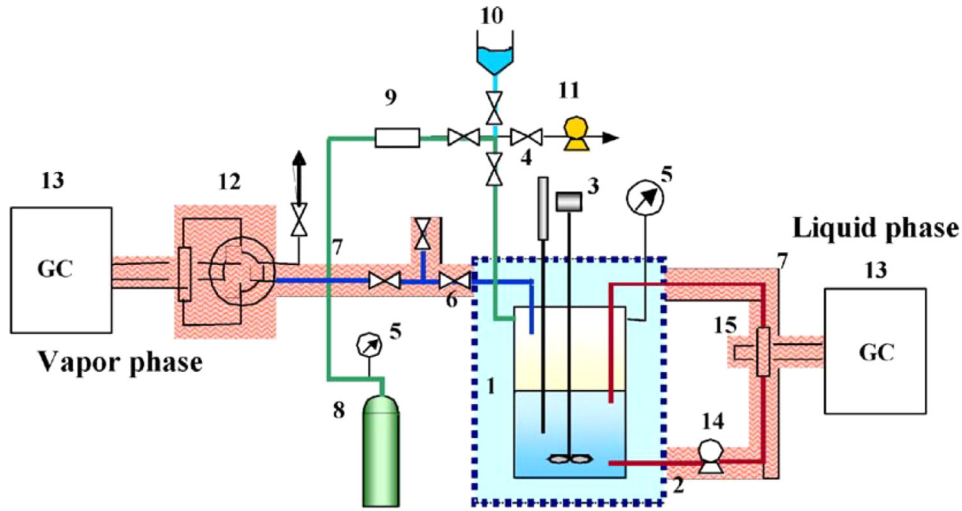$$P = \frac{RT}{v - b} - \frac{a(T)}{v(v + b) + b(v - b)} \tag{1}$$

Fig. 2. Schematic diagram of the experimental apparatus for measuring isothermal VLE. 1, equilibrium cell; 2, water bath; 3, stirrer; 4, thermometer; 5, pressure indicator; 6, sampling valve; 7, ribbon heater; 8, CO_2 cylinder; 9, in-line filter; 10, sample installation; 11, vacuum pump; 12, six-way valve; 13, gas chromatograph; 14, circulation pump; and 15, sample injector.

where P is the pressure, R is the ideal gas constant, T is the temperature, v is the molar volume, a is the energy parameter and b is the size parameter. These parameters for pure components i, were calculated using

$$a_{ii}(T) = \frac{0.45724R^2T_{c,i}^2}{P_{c,i}}\left[1 + m_i\left(1 - \sqrt{\frac{T}{T_{c,i}}}\right)\right]^2 \quad (2)$$

$$m_i = 0.37464 + 1.5422\omega_i - 0.26992\omega_i^2 \quad (3)$$

and

$$b_i = \frac{0.07780RT_{c,i}}{P_{c,i}} \quad (4)$$

where $T_{c,i}$ and $P_{c,i}$ are the critical temperature and critical pressure for pure component, respectively, and ω_i is the acentric factor. The pure component parameters $T_{c,i}$, $P_{c,i}$ and ω_i [11,42,43] used to calculate the a and b values for the pure components CO_2, HFE-449mec-f, or HFE-7200 are provided in Table 4. The acentric factor, ω_i, for HFE-449mec-f and HFE-7200 was estimated from pressure-temperature data.

The vdW1 and WS mixing rules were used to calculate the mixture energy parameter, a, and the size parameter, b. The vdW1 mixing rule is given by,

$$a = \sum_{i=1}^{NC}\sum_{j=1}^{NC} x_i x_j \left(a_{ii}a_{jj}\right)^{0.5}\left(1 - k_{ij}\right)$$
$$\left(k_{ij} = k_{ji}, \quad k_{ii} = k_{jj} = 0\right) \quad (5)$$

and

$$b = \sum_{i=1}^{NC} x_i x_j \left(\frac{b_i + b_j}{2}\right)\left(1 - l_{ij}\right)$$
$$\left(l_{ij} = l_{ji}, \quad l_{ii} = l_{jj} = 0\right) \quad (6)$$

where k_{ij} and l_{ij} are binary interaction parameters. The WS mixing rule for the PR EOS is given by,

$$\frac{a}{b} = \sum_{i=1}^{NC} x_i \frac{a_{ii}}{b_i} + \frac{A_\infty^E}{C} \quad (7)$$

$$b = \frac{\sum_{i=1}^{NC}\sum_{j=1}^{NC} x_i x_j \left(b - \frac{a}{RT}\right)_{ij}}{1 - \sum_{i=1}^{NC} x_i \frac{a_{ii}}{bRT} - \frac{A_\infty^E}{CRT}} \quad (8)$$

$$\left(b - \frac{a}{RT}\right)_{ij} = \frac{1}{2}\left[\left(b_i - \frac{a_{ii}}{RT}\right) + \left(b_j - \frac{a_{jj}}{RT}\right)\right]\left(1 - k_{ij}\right)$$
$$\left(k_{ij} = k_{ji}, \quad k_{ii} = k_{jj} = 0\right) \quad (9)$$

with the constant C in Eq. (8) as

$$C = \frac{\ln\left(\sqrt{2} - 1\right)}{\sqrt{2}} \quad (10)$$

where A_∞^E is the excess Helmholtz free energy at infinite pressure, and k_{ij} is the second virial coefficient binary interaction parameter. The NRTL model [27] was applied to calculate A_∞^E given by,

$$A_\infty^E = \sum_{i=1}^{NC} x_i \frac{\sum_{j=1}^{NC} x_j \tau_{ji} G_{ji}}{\sum_{k=1}^{NC} x_k G_{ki}} \quad (11)$$

$$G_{ij} = \exp\left(-\alpha_{ij}\tau_{ij}\right) \quad \left(\alpha_{ij} = \alpha_{ji}, \quad \alpha_{ii} = \alpha_{jj} = 0\right) \quad (12)$$

$$\tau_{ij} = \frac{g_{ij} - g_{jj}}{RT} \quad \left(\tau_{ii} = \tau_{jj} = 0\right) \quad (13)$$

where $g_{ij} - g_{jj}$ is the binary interaction parameter of the NRTL model. The value of 0.3 was used for α_{12} according to recommendation by Renon and Prausnitz [27]. k_{12} and l_{12} in the vdW1 mixing rule, and k_{12}, $g_{12} - g_{22}$ and $g_{21} - g_{11}$ in the WS-NRTL mixing rule were treated as fitted parameters, and were regressed by minimizing the following objective function (F_{obj}):

$$F_{obj} = \sum_{k=1}^{NDP}\left(\frac{P_{exptl.} - P_{calcd.}}{P_{exptl.}}\right)_k^2 \quad (14)$$

where NDP is the number of experimental data points, and "exptl." and "calcd." are the experimental and calculated values, respectively.

3.2. GC-SAFT-VR

In the GC-SAFT-VR approach [28], the functional groups in molecules are represented by tangentially bonded segments that each have individual size and energy parameters. The functional group i in molecule k interacts with functional group j in molecule l through dispersive interactions via the square-well potential as

described by,

$$u_{ki,lj}(r) = \begin{cases} +\infty & \text{if } r < \sigma_{ki,lj} \\ -\varepsilon_{ki,lj} & \text{if } \sigma_{ki,lj} \le r \le \lambda_{ki,lj}\sigma_{ki,lj} \\ 0 & \text{if } r > \lambda_{ki,lj}\sigma_{ki,lj} \end{cases} \quad (15)$$

where r is the distance between the two groups, $\sigma_{ki,lj}$ is the segment diameter, and $\varepsilon_{ki,lj}$ and $\lambda_{ki,lj}$ are the dispersion energy well depth and range parameters, respectively. The cross interactions for size and energy between unlike segments can be expressed by Lorentz-Berthelot combining rules,

$$\sigma_{ki,lj} = \frac{\sigma_{ki,ki} + \sigma_{lj,lj}}{2} \quad (16)$$

$$\varepsilon_{ki,lj} = \xi_{ki,lj}\sqrt{\varepsilon_{ki,ki}\varepsilon_{lj,lj}} \quad (17)$$

$$\lambda_{ki,lj} = \gamma_{ki,lj}\left(\frac{\sigma_{ki,ki}\lambda_{ki,ki} + \sigma_{lj,lj}\lambda_{lj,lj}}{\sigma_{ki,ki} + \sigma_{lj,lj}} \right) \quad (18)$$

where $\xi_{ki,lj}$ and $\gamma_{ki,lj}$ are binary interaction parameters that enable adjustments to the cross interactions from the geometric and arithmetic mean values, respectively.

The definition if the Helmholtz free energy for a non-associating fluid in the GC-SAFT-VR approach is given by,

$$\frac{A}{Nk_BT} = \frac{A^{\text{ideal}}}{Nk_BT} + \frac{A^{\text{mono}}}{Nk_BT} + \frac{A^{\text{chain}}}{Nk_BT} \quad (19)$$

where N is the total number of molecules in the system, k_B is the Boltzmann constant, T is the absolute temperature, A^{ideal}, A^{mono}, and A^{chain} are the contributions to the Helmholtz free energy from the ideal, monomer, and hetero-segmented chain interactions, respectively. The reader is referred to the original publications [28,44] for details of the terms in Eq. (19), here we provide only the main expressions and a brief description of each term.

The ideal contribution to the Helmholtz free energy is given by,

$$\frac{A^{\text{ideal}}}{Nk_BT} = \sum_{k=1}^{n_{\text{components}}} x_k \ln\left(\rho_k \Lambda_k^{3}\right) - 1 \quad (20)$$

where $n_{\text{components}}$ represents the number of pure components in the system, x_k is the mole fraction of component k, ρ_k is the molecular number density, N_k/V, where N_k is the number of molecules of component k and V is the volume of the system, and Λ_k is the de Broglie wavelength of component k.

The monomer contribution to the Helmholtz free energy is given by the temperature expansion of the second order Barker Henderson perturbation theory for mixtures [45],

$$\frac{A^{\text{mono}}}{Nk_BT} = \sum_{k=1}^{n} \sum_{i=1}^{n'_k} m_{ki} x_k \left(a^{\text{HS}} + \frac{a_1}{k_BT} + \frac{a_2}{(k_BT)^2} \right) \quad (21)$$

where n'_k is the number of types of functional groups i in a chain of component k and m_{ki} is the number of segments of type i in chains of component k. a^{HS}, a_1, and a_2 represent the hard-sphere reference term and the first and second order perturbation terms, respectively.

Finally, the contribution to the Helmholtz free energy from chain formation from the hetero-segmented monomer fluid is represented by,

$$\frac{A^{\text{chain}}}{Nk_BT} = -\sum_{k=1}^{n} x_k \sum_{ij} \ln y_{ki,kj}^{\text{SW}}\left(\sigma_{ki,kj}\right) \quad (22)$$

where the first sum is over all of the components, n, in the mixture, x_k is again the mole fraction of component k, the second

Table 2

Experimental isothermal VLE data for the system CO_2 (1) + HFE-449mec-f (2) at temperatures (T) 303.15, 313.15, and 323.15 K. Pressure (P), liquid mole fraction (x_1), and vapor mole fraction (y_1). Standard uncertainties, u, are $u(T) = 0.1$ K, $u(P) = 0.03$ MPa, $u(x_1) = 0.007$, and $u(y_1) = 0.007$.

P (MPa)	x_1	y_1	P (MPa)	x_1	y_1
$T = 303.15$ K					
0.540	0.177	0.936	4.064	0.774	0.997
1.582	0.427	0.984	4.474	0.812	0.996
2.101	0.521	0.995	4.999	0.856	0.997
2.500	0.585	0.997	5.475	0.893	0.998
3.027	0.656	0.996	6.082	0.932	0.996
3.512	0.715	0.996			
$T = 313.15$ K					
0.602	0.167	0.955	4.874	0.780	0.995
0.970	0.253	0.977	5.447	0.824	0.995
1.669	0.396	0.984	6.126	0.869	0.992
1.911	0.437	0.987	6.417	0.888	0.990
2.454	0.521	0.992	6.841	0.911	0.993
2.979	0.590	0.993	7.584	0.951	0.996
3.370	0.636	0.991	8.022	0.974	0.996
3.802	0.681	0.997	8.118	0.974	0.991
4.352	0.733	0.994			
$T = 323.15$ K					
0.754	0.179	0.976	4.894	0.713	0.990
1.090	0.248	0.975	5.432	0.762	0.992
2.014	0.407	0.985	6.241	0.805	0.992
2.343	0.457	0.988	6.612	0.835	0.992
2.949	0.534	0.988	7.128	0.857	0.992
3.487	0.594	0.989	7.655	0.885	0.987
3.990	0.644	0.993	7.999	0.910	0.987
4.547	0.694	0.991			

sum considers the chain formation and the connectivity of the segments within a given component k. The background correlation function $y_{ki,kj}^{\text{SW}}$ is given by.

$$y_{ki,kj}^{\text{SW}}\left(\sigma_{ki,kj}\right) = \exp\left(\frac{-\varepsilon_{ki,kj}}{k_BT} \right) g_{ki,kj}^{\text{SW}}\left(\sigma_{ki,kj}\right) \quad (23)$$

where $\varepsilon_{ki,kj}$ is the segment-segment dispersion energy well depth and $g_{ki,kj}^{\text{SW}}(\sigma_{ki,kj})$ is the radial distribution function for the square-well monomers at the contact distance of $\sigma_{ki,kj}$ and is approximated by a first-order high temperature expansion [29].

Once the Helmholtz free energy is obtained, other thermodynamic properties, such as chemical potential and pressure can be calculated through standard thermodynamic relationships.

4. Results and discussion

4.1. Experimental VLE data for the binary systems CO_2 + HFE-449mec-f or HFE-7200

VLE data for the binary systems CO_2 (1) + HFE-449mec-f or HFE-7200 (2) were measured at temperatures 303.15, 313.15, and 323.15 K. The experimental VLE data are listed in Tables 2 and 3, respectively. Again, HFE-7200 is a binary mixture of two isomers with mole fraction of 0.614 for CAS number 163702-06-5 and 0.386 for CAS 163702-05-4, as mentioned in the Materials section. Plots of pressure (P) as functions of the liquid or vapor mole fraction of CO_2 (x_1 or y_1) for two systems are also presented in Figs. 3 and 4, respectively. The pressure was measured up to about 8.6 MPa in this work. To our best knowledge, the experimental VLE data of these systems have not been previously reported in the literature. A comparison of Figs. 3 and 4 shows that the P-x_1 diagram of the system CO_2 + HFE-7200, which has a higher carbon number, shifts to higher pressures, compared to the CO_2 + HFE-449mec-f system.
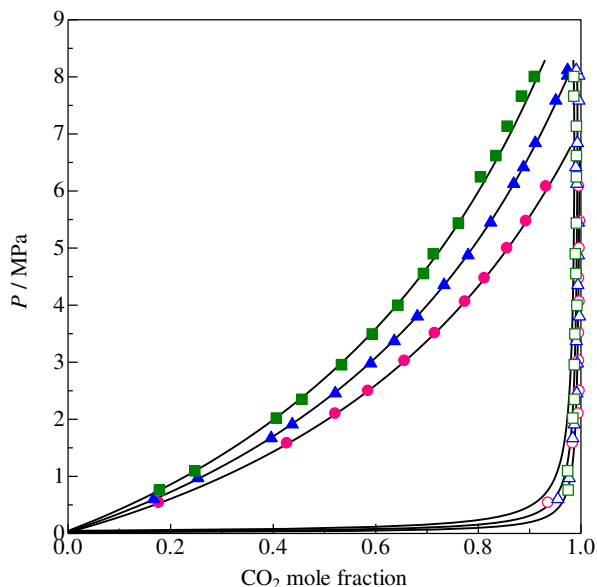
Fig. 3. Experimental VLE data for the system CO_2 (1) + HFE-449mec-f (2) at 303.15, 313.15, and 323.15 K. Experimental data at liquid phase; ● 303.15 K; ▲ 313.15 K; ■ 323.15 K, vapor phase; ○ 303.15 K; △ 313.15 K; □ 323.15 K. Results obtained from — PR EOS with vdW1 mixing rule.
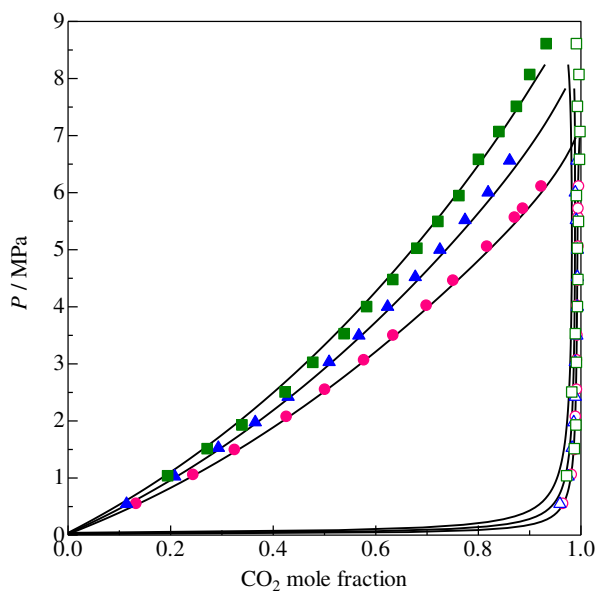

Fig. 4. Experimental VLE data for the system CO_2 (1) + HFE-7200 (2) at 303.15, 313.15, and 323.15 K. Experimental data at liquid phase; ● 303.15 K; ▲ 313.15 K; ■ 323.15 K, vapor phase; ○ 303.15 K; △ 313.15 K; □ 323.15 K. Results obtained from — PR EOS with vdW1 mixing rule.

Table 3

Experimental isothermal VLE data for the system CO_2 (1) + HFE-7200 (2) at temperatures (T) 303.15, 313.15, and 323.15 K. Pressure (P), liquid mole fraction (x_1), and vapor mole fraction (y_1). Standard uncertainties, u, are $u(T) = 0.1$ K, $u(P) = 0.03$ MPa, $u(x_1) = 0.007$, and $u(y_1) = 0.007$. HFE-7200 is a binary mixture of two isomers with mole fraction of 0.614 for CAS number 163702-06-5 and 0.386 for CAS 163702-05-4, with a standard uncertainty $u(x) = 0.01$.

P (MPa)	x_1	y_1	P (MPa)	x_1	y_1
T = 303.15 K					
0.550	0.133	0.965	4.020	0.699	0.993
1.057	0.244	0.982	4.460	0.751	0.994
1.493	0.325	0.988	5.056	0.817	0.995
2.074	0.426	0.990	5.565	0.871	0.995
2.549	0.501	0.992	5.722	0.887	0.995
3.065	0.577	0.992	6.110	0.923	0.996
3.499	0.634	0.993			
T = 313.15 K					
0.546	0.114	0.959	4.001	0.623	0.993
1.027	0.208	0.975	4.522	0.677	0.993
1.529	0.293	0.983	5.000	0.725	0.993
1.977	0.365	0.986	5.520	0.774	0.991
2.424	0.429	0.989	6.003	0.819	0.989
3.033	0.509	0.989	6.562	0.861	0.992
3.497	0.567	0.992			
T = 323.15 K					
1.032	0.195	0.973	5.019	0.681	0.994
1.507	0.272	0.988	5.489	0.722	0.996
1.922	0.340	0.991	5.941	0.763	0.992
2.500	0.424	0.983	6.577	0.801	0.998
3.020	0.478	0.992	7.063	0.841	0.999
3.522	0.539	0.990	7.505	0.875	0.994
3.996	0.583	0.994	8.063	0.901	0.997
4.471	0.634	0.995	8.603	0.933	0.992

4.2. Correlation

The determined parameters in both mixing rules along with the percentage average relative deviations of the experimental and calculated P, $|\Delta P/P|_{av.}$ and the average absolute deviations of the experimental and calculated y_1, $|\Delta y_1|_{av.}$, are provided in Table 5. These parameters were determined per system and are temperature independent. The vdW1 mixing rule gave $|\Delta P/P|_{av.} \times 100$ and $|\Delta y_1|_{av.}$ of less than 2.9% and 0.017, respectively for each dataset, whilst using the WS-NRTL mixing rule resulted in values of 3.1% and 0.012. Thus, both models show reasonable correlation of the results at all temperatures investigated. Figs. 5 and 6 shows the relative deviations between the experimental and calculated P defined as $(P_{exptl.} - P_{calcd.})/P_{exptl.} \times 100$ (%), and the absolute deviation between the experimental and calculated y_1 defined as $y_{1,exptl.} - y_{1,calcd.}$, as a function of liquid phase CO_2 mole fraction, x_1 in the systems CO_2 + HFE-449mec-f and CO_2 + HFE-7200, respectively. The values of $(P_{exptl.} - P_{calcd.})/P_{exptl.} \times 100$ (%) and $y_{1,exptl.} - y_{1,calcd.}$ were generally within the uncertainties of the experimental pressure and vapor-phase mole fraction for both models; however, higher values were detected in some data of both systems, espe-

Table 4

Critical temperature, T_c, critical pressure, P_c, acentric factor, ω, and Antoine constants, A, B, C values for the pure components.

Component	T_c (K)	P_c (MPa)	ω	Antoine A [a]	Antoine B [a]	Antoine C [a]
CO_2	304.12 [b]	7.374 [b]	0.225 [b]			
HFE-449mec-f	475.74 [c]	2.233 [c]	0.529 [d]	6.08992 [e]	1126.735 [e]	-69.161 [e]
HFE-7200	483.00 [f]	2.007 [f]	0.464 [d]	6.19053 [f]	1243.910 [f]	-52.285 [f]

[a] $\log (P_i^s/kPa) = A - B/[(T/K) + C]$.
[b] Poling et al. [11].
[c] Yasumoto et al. [3].
[d] Estimated by the definition of acentric factor: $\omega = -\log(P_r^s)_{T_r=0.7} - 1$, which P_r^s is P_i^s/P_c.
[e] Tochigi et al. [42].
[f] Dortmund Data Bank 2019 [43].

Table 5

Parameters and deviations between the calculated and experimental pressures ($|\Delta P/P|$)[a] and vapor phase mole fractions ($|\Delta y_1|$)[b], for the PR EOS combined with the vdW1 and WS-NRTL mixing rules and for the GC-SAFT-VR EOS both with and without the adjusted CO_2-CF_2 cross-interaction for the systems CO_2 (1) + HFE-449mec-f (2) and CO_2 (1) + HFE-7200 (2).

	CO_2 (1) + HFE-449mec-f (2)			CO_2 (1) + HFE-7200 (2)		
	303.15 K	313.15 K	323.15 K	303.15 K	313.15 K	323.15 K
Parameters of vdW1 mixing rule						
	$k_{12} = -0.0516$, $l_{12} = 0.0436$			$k_{12} = 0.0322$, $l_{12} = 0.0430$		
$|\Delta P/P|_{av.} \times 100$ (%)	0.6	0.6	1.5	1.6	2.2	2.9
$|\Delta y_1|_{av.}$	0.005	0.004	0.009	0.001	0.005	0.017
Parameters of WS-NRTL mixing rule						
	$g_{12} - g_{22}$ (J mol^{-1}) = 1604.893, $g_{21} - g_{11}$ (J mol^{-1}) = −2039.110			$g_{12} - g_{22}$ (J mol^{-1}) = 5130.300, $g_{21} - g_{11}$ (J mol^{-1}) = −2325.171		
	$k_{12} = 0.4839$, $\alpha_{12} = 0.3$			$k_{12} = 0.5940$, $\alpha_{12} = 0.3$		
$|\Delta P/P|_{av.} \times 100$ (%)	0.5	0.6	1.2	1.9	2.0	3.1
$|\Delta y_1|_{av.}$	0.005	0.004	0.009	0.001	0.004	0.012
GC-SAFT-VR						
$|\Delta P/P|_{av.} \times 100$ (%)	0.08	0.08	0.09	0.07	0.10	0.07
$|\Delta y_1|_{av.}$	0.007	0.014	0.017	0.094	0.100	0.065
GC-SAFT-VR with adjusted CO_2-CF_2 cross-interaction						
$|\Delta P/P|_{av.} \times 100$ (%)	0.09	0.07	0.09	0.08	0.09	0.08
$|\Delta y_1|_{av.}$	0.044	0.046	0.053	0.007	0.008	0.034

[a] $|\Delta P/P|_{av.} \times 100 = (100/NDP) \sum_{k=1}^{NDP} |(P_{exptl.} - P_{calcd.})/P_{exptl.}|_k$

[b] $|\Delta y_1|_{av.} = \sum_{k=1}^{NDP} |y_{1,exptl.} - y_{1,calcd.}|_k/NDP$, where NDP is the number of data points.
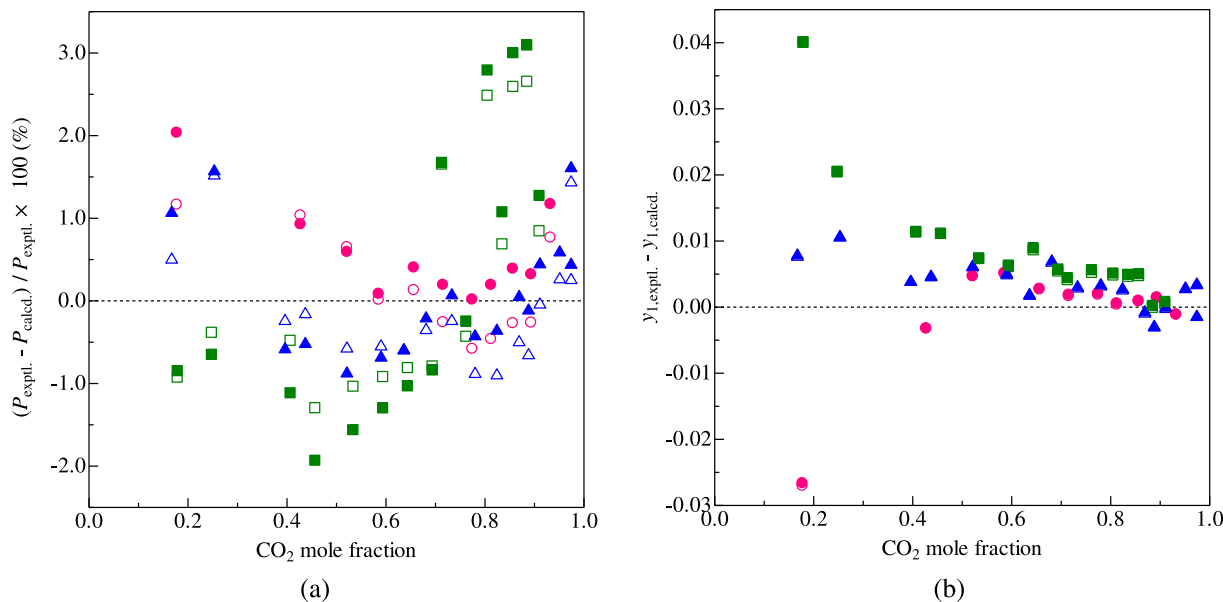

Fig. 5. Relative deviations between the experimental and calculated results vs. CO_2 mole fraction for the system CO_2 (1) + HFE-449mec-f (2). PR EOS with vdW1 mixing rule at ● 303.15 K; ▲ 313.15 K; ■ 323.15 K. PR EOS with WS-NRTL mixing rule at ○ 303.15 K; △ 313.15 K; □ 323.15 K. (a) $(P_{exptl.} - P_{calcd.})/P_{exptl.} \times 100$ (%) and (b) $y_{1,exptl.} - y_{1,calcd.}$.

cially at temperature 323.15 K. The results of calculations using the vdW1 and WS-NRTL mixing rules are summarized graphically in Figs. 3 and 4.

4.3. Prediction using the GC-SAFT-VR

As shown in Fig. 1, where each functional group is circled, HFE-449mec-f and HFE-7200 are both composed of CF_3, CF_2, CHF, CH_3, and ether CH_2O groups. The parameters for these functional groups were taken from previous work [5,28,30] and reported for completeness in Tables 6–8. Since CO_2 is a small molecule, it is not broken up into individual groups and represented by the SAFT-VR parameters proposed by Ramos et al. [46] as reported in Tables 6–8. Using these parameters, an average absolute deviation in the pressure ($|\Delta P/P|_{av.}$ %) for pure HFE-7200 of 2.02% and 19.35% for

Table 6

GC-SAFT-VR parameters for the segment size, σ, and number, m, parameters for each of the groups studied.

Groups	σ_i (Å)	m_i
CO_2	2.774	2.000
CF_3	4.618	0.685
CF_2	4.345	0.370
OCH_2 (ether)	3.124	1.000
CHF	3.962	0.548
CH_3	3.737	0.667

pure HFE-449mec-f compared to experimental data [3] are obtained. Likely, the high $|\Delta P/P|_{av.}$ % value for pure HFE-449mec-f is due to the additional CF_3 functional group present in the HFE-
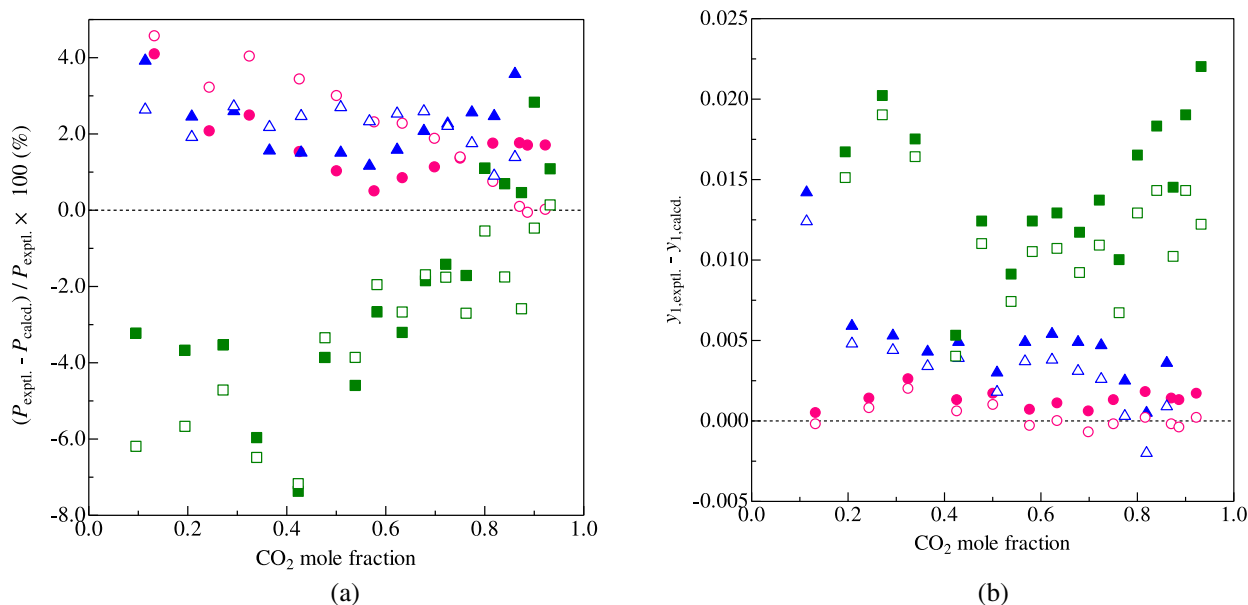
Fig. 6. Relative deviations between the experimental and calculated results vs. CO_2 mole fraction for the system CO_2 (1) + HFE-7200 (2). PR EOS with vdW1 mixing rule at ● 303.15 K; ▲ 313.15 K; ■ 313.15 K. PR EOS with WS-NRTL mixing rule at ○ 303.15 K; △ 313.15 K; □ 323.15 K. (a) $(P_{exptl.} - P_{calcd.})/P_{exptl.} \times 100$ (%) and (b) $y_{1,exptl.} - y_{1,calcd.}$.
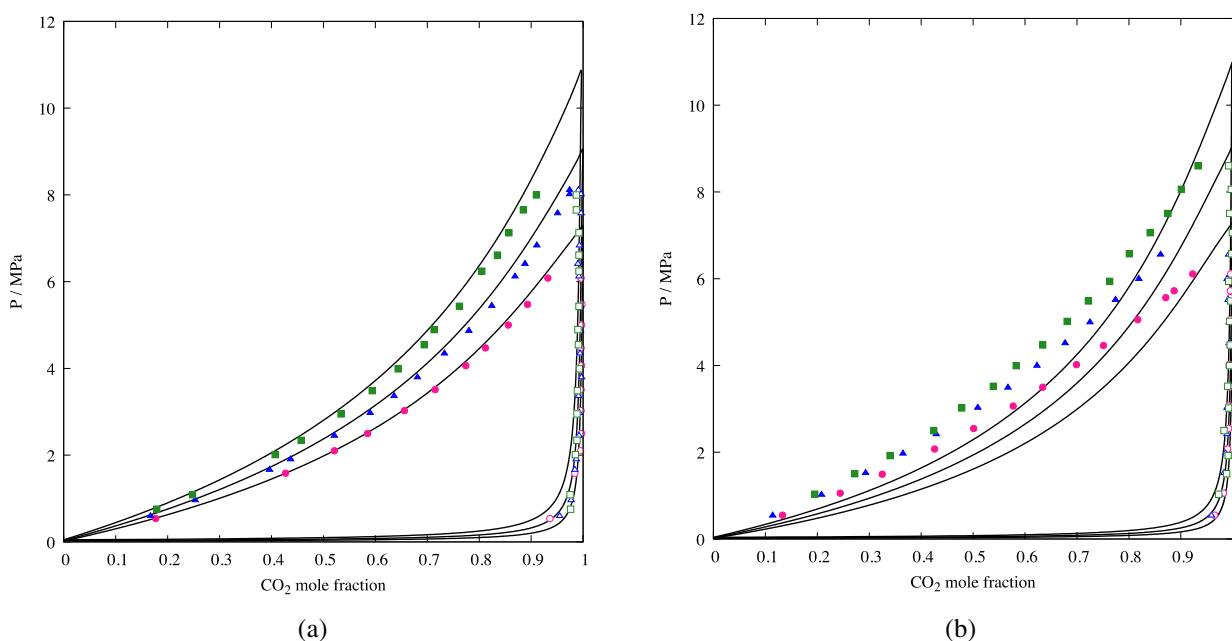
Fig. 7. Px slices of (a) CO_2 (1) + HFE-449mec-f (2) and (b) CO_2 (1) + HFE-7200 (2) at constant temperatures of 303.15, 313.15, and 323.15 K. Solid lines correspond to predictions from the GC-SAFT-VR approach. Points correspond to experimental data presented here at liquid phase: ● 303.15 K, ▲ 313.15 K, ■ 323.15 K, and vapor phase: ○ 303.15 K, △ 313.15 K, □ 323.15 K.

449mec-f molecule, instead of the smaller CH_3 functional group in HFE-7200. In Fig. 7 (a) and (b) respectively the constant temperature predictions of the CO_2 + HFE-449mec-f and CO_2 + HFE-7200 phase diagrams at 303.15, 313.15, and 323.15 K are shown. From the figures, it can be seen that the predictions are in good agreement with the experimental data, specifically for the CO_2 + HFE-449mec-f mixture (Fig. 7(a)). In order to quantitatively compare the experimental mixture data to the GC-SAFT-VR predictions, the average absolute deviation in the vapor phase mole fraction of CO_2 ($|\Delta y_1|_{av.}$) are reported in Table 5 along with the $|\Delta P/P|_{av}$ % values for the mixtures at 303.15, 313.15, 323.15 K. The $|\Delta y_1|_{av.}$ values are averaged across the 3 examined temperatures and devia-

tions of 0.012 and 0.086 are obtained for the CO_2 + HFE-449mec-f and CO_2 + HFE-7200 systems, respectively. We note that this fit is purely predictive, since all parameters were obtained from a fit to pure component data, which is one of the advantages of using a group-contribution based SAFT approach. However, since the molecule set used to determine the interactions in fluorinated ether systems in the work of Haley et al. [5] was small, the use of an adjusted cross interaction between CO_2 and the CF_2 group was investigated to see if a better prediction of the CO_2 + HFE-7200 mixture could be obtained. The optimized cross interaction was fitted to the CO_2 + HFE-7200 system at 303.15 K and is reported in reported in Tables 7 and 8. Although, the adjustment of
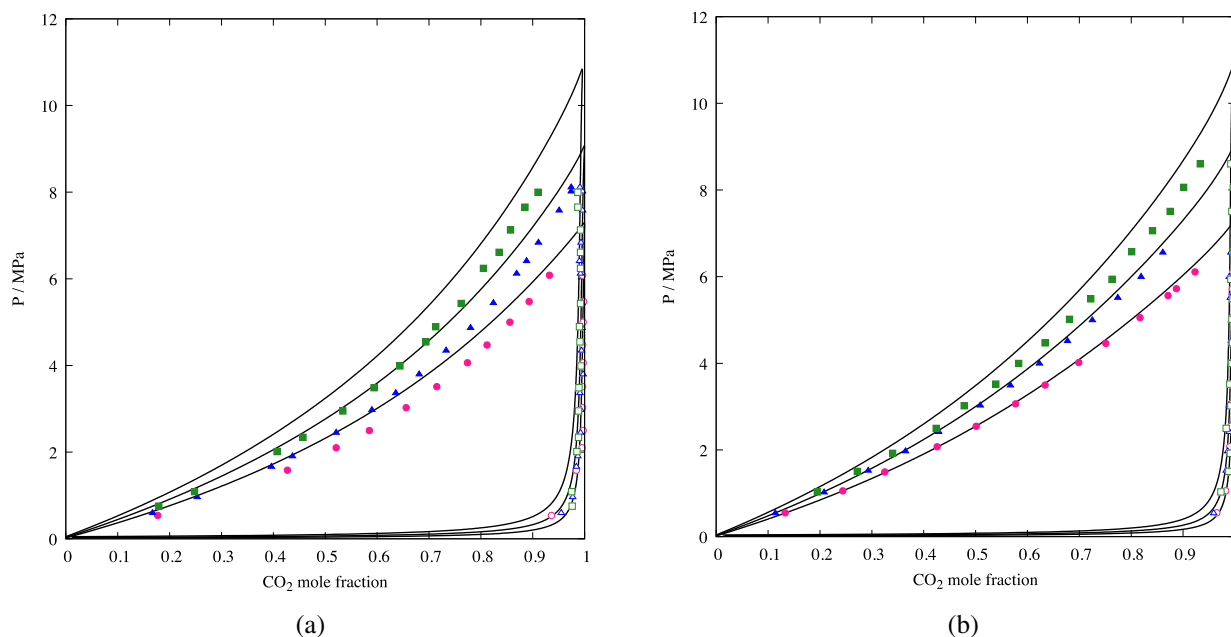
Fig. 8. *Px* slices of (a) CO_2 (1) + HFE-449mec-f (2) and (b) CO_2 (1) + HFE-7200 (2) at constant temperatures of 303.15, 313.15, and 323.15 K with a binary interaction parameter between CO_2 and CF_2. Solid lines correspond to predictions from the GC-SAFT-VR approach. Points correspond to experimental data presented here at liquid phase: ● 303.15 K, ▲ 313.15 K, ■ 323.15 K, and vapor phase: ○ 303.15 K, △ 313.15 K, □ 323.15 K.

Table 7
GC-SAFT-VR segment-segment dispersion energy range parameters $\lambda_{ki,lj}$.

	CO_2	CF_3	CF_2	OCH_2 (ether)	CHF	CH_3
CO_2	1.527	1.398	1.597	1.613	1.425	1.507
CF_3	1.398	1.321	1.476	1.470	1.336	1.398
CF_2	1.597	1.476	1.641	1.694	1.504	1.572
OCH_2 (ether)	1.613	1.470	1.694	1.690	1.502	1.582
CHF	1.425	1.336	1.504	1.502	1.354	–
CH_3	1.507	1.398	1.572	1.582	–	1.492

Note that these parameters differ from Haley et al. [5] due to a table misprint.

this cross interaction away from the Lorentz-Berthelot value has a minimal effect on the CO_2 + HFE-449mec-f mixture ($|\Delta y_1|_{av.}$ of 0.012 to 0.047), as shown in Fig. 8 (a), it significantly improves the agreement with experimental data for the CO_2 + HFE-7200 system ($|\Delta y_1|_{av.}$ of 0.086 to 0.016) as can be seen in Fig. 8 (b) and reported in Table 5. Note that the cross interaction between CO_2 and CF_2 was fitted using the $|\Delta y_1|_{av.}$ values because of the small to nonexistent changes in the $|\Delta P/P|_{av.}$ % values.

Finally, the *p,T* projection of the fluid phase diagram was predicted for both mixtures with the parameter set that includes the optimized CO_2–CF_2 cross interaction and can be seen in Fig. 9. As can be seen from the figure type I phase behavior is found according to the scheme of Scott and van Konynenburg [47]. We note that both sets of parameters, i.e., with and without the adjusted CO_2–CF_2 cross interaction yield very similar phase diagrams. The GC-
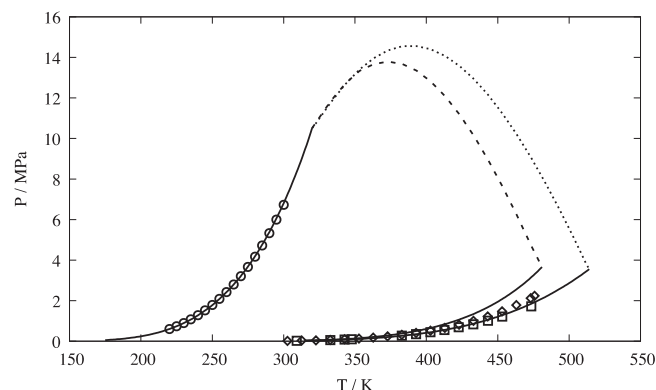

Fig. 9. Projected pressure-temperature diagram of HFE-449mec-f + CO_2 (‒‒‒) and HFE-7200 + CO_2 (······) where the dotted lines represent the GC-SAFT-VR predicted critical line of both the mixtures utilizing the CO_2-CF_2 binary interaction parameter, the experimental data [3,48] for the pure components are shown as open symbols for CO_2 (○), HFE-449mec-f (◇), and HFE-7200 (□), and the solid lines are the GC-SAFT-VR predictions for the pure components presented here.

SAFT-VR approach, like all analytical equations of state, over predicts the critical point [49–52] and so the predicted critical line is likely somewhat higher than the experimental values; however, we anticipate the type of phase diagram to be unaffected.

Table 8
GC-SAFT-VR segment-segment dispersion energy well depth parameters $\varepsilon_{ki,lj} / k_B$ (K).

	CO_2	CF_3	CF_2	OCH_2 (ether)	CHF	CH_3
CO_2	179.32	237.87	162.45	179.79	287.82	204.95
CF_3	237.87	315.56	262.81	238.50	381.81	271.88
CF_2	162.45	262.81	218.87	158.91	317.99	226.43
OCH_2 (ether)	179.79	238.50	158.91	180.27	288.58	205.49
CHF	287.82	381.81	317.99	288.58	461.98	–
CH_3	204.95	271.88	226.43	205.49	–	234.25

Note that these parameters differ from Haley et al. [5] due to a table misprint.

5. Conclusions

The experimental VLE data were obtained for two binary systems CO_2 + HFE-449mec-f or HFE-7200 at temperatures 303.15, 313.15, and 323.15 K and at pressure up to 9.0 MPa. This study furthers our understanding of these refrigerant mixtures as no experimental data were previously available for these two binary systems. The experimental VLE data were well correlated by the PR EOS with the vdW1and WS-NRTL mixing rules. These models provide reasonable agreements with the experimental data. The GC-SAFT-VR approach was also found to be able to correctly predict the phase behavior of the CO_2 + HFE binary mixtures. Due to the molecular polarity of the HFEs studied, optimization of the cross interaction between CO_2 and CF_2 was found to allow for better representation of the phase behavior than using Lorentz-Berthelot combining rules alone. Utilizing the fitted cross interaction the full phase diagram of the CO_2 + HFE-449mec-f and CO_2 + HFE-7200 systems was also predicted and type 1 phase behavior observed.

Declaration of Competing Interest

None.

CRediT authorship contribution statement

Hiroyuki Matsuda: Conceptualization, Data curation, Formal analysis, Methodology, Project administration, Resources, Supervision, Writing - original draft. **Toru Suga:** Data curation, Investigation. **Tomoya Tsuji:** Formal analysis, Validation. **Katsumi Tochigi:** Methodology, Visualization. **Kiyofumi Kurihara:** Funding acquisition, Validation, Writing - review & editing. **Alyssa K. Nelson:** Data curation, Formal analysis, Investigation, Software, Writing - original draft. **Clare McCabe:** Conceptualization, Methodology, Funding acquisition, Supervision, Writing - review & editing.

Acknowledgements

References

[1] W.-T. Tsai, J. Hazard. Mater. 119 (2005) 69–78, doi:10.1016/j.jhazmat.2004.12.018.

[2] A. Sekiya, S. Misaki, J. Fluor. Chem. 101 (2000) 215–221, doi:10.1016/S0022-1139(99)00162-1.

[3] M. Yasumoto, Y. Yamada, J. Murata, S. Urata, K. Otake, J. Chem. Eng. Data 48 (2003) 1368–1379, doi:10.1021/je0201976.

[4] Y. Uchida, M. Yasumoto, Y. Yamada, K. Ochi, T. Furuya, K. Otake, J. Chem. Eng. Data 49 (2004) 1615–1621, doi:10.1021/je0499723.

[5] J.D. Haley, C. McCabe, Fluid Phase Equilib. 440 (2017) 111–121, doi:10.1016/j.fluid.2017.01.013.

[6] D. Fang, Y. Li, X. Meng, J. Wu, J. Chem. Thermodyn. 69 (2014) 36–42, doi:10.1016/j.jct.2013.09.035.

[7] M.H. Rausch, L. Kretschmer, S. Will, A. Leipertz, A.P. Fröba, J. Chem. Eng. Data 60 (2015) 3759–3765, doi:10.1021/acs.jced.5b00691.

[8] C.G. Albà, L.F. Vega, F. Llovell, Int. J. Refrig. 113 (2020) 145–155, doi:10.1016/j.ijrefrig.2020.01.008.

[9] W.A. Fouad, L.F. Vega, AIChE J. 64 (2018) 250–262, doi:10.1002/aic.15859.

[10] P. Nekså, Int. J. Refrig. 25 (2002) 421–427, doi:10.1016/S0140-7007(01)00033-0.

[11] B.E. Poling, J.M. Prausnitz, J.P. O'Connell, The Properties of Gases and Liquids, 5th ed., McGraw-Hill, New York, 2001.

[12] R. Akasaka, J. Therm. Sci. Tech.-Jpn. 4 (2009) 159–168, doi:10.1299/jtst.4.159.

[13] K. Djebaili, E.E. Ahmar, A. Valtz, A.H. Meniai, C. Coquelet, J. Chem. Eng. Data 63 (2018) 4626–4631, doi:10.1021/acs.jced.8b00683.

[14] G. Silva-Oliver, L.A. Galicia-Luna, Fluid Phase Equilib. 199 (2002) 213–222, doi:10.1016/S0378-3812(01)00816-0.

[15] C. Duran-Valencia, G. Pointurier, A. Valtz, P. Guilbot, D. Richon, J. Chem. Eng. Data 47 (2002) 59–61, doi:10.1021/je010075y.

[16] A.M.A. Dias, H. Carrier, J.L. Daridon, J.C. Pàmies, L.F. Vega, J.A.P. Coutinho, I.M. Marrucho, Ind. Eng. Chem. Res. 45 (2006) 2341–2350, doi:10.1021/ie051017z.

[17] J.S. Lim, J.M. Jin, K.-P. Yoo, J. Supercrit. Fluids 44 (2008) 279–283, doi:10.1016/j.supflu.2007.09.025.

[18] S.A. Kim, J.S. Lim, J.W. Kang, J. Chem. Eng. Data 55 (2010) 4999–5003, doi:10.1021/je100583z.

[19] G. Raabe, J. Chem. Eng. Data 58 (2013) 1867–1873, doi:10.1021/je4002619.

[20] S.A. Gornati, D.D. Bona, P. Chiesa, Fluid Phase Equilib. 498 (2019) 94–103, doi:10.1016/j.fluid.2019.06.024.

[21] K. Tochigi, T. Namae, T. Suga, H. Matsuda, K. Kurihara, M.C. dos Ramos, C. McCabe, J. Supercrit. Fluids 55 (2010) 682–689, doi:10.1016/j.supflu.2010.10.016.

[22] S. Urata, A. Takada, T. Uchimaru, A.K. Chandra, Chem. Phys. Lett. 368 (2003) 215–223, doi:10.1016/S0009-2614(02)01718-9.

[23] R.C. Deka, B.K. Mishra, J. Mol. Graph. Model. 53 (2014) 23–30, doi:10.1016/j.jmgm.2014.07.003.

[24] 3M Novec 7200 Engineered Fluid Datasheet, http://multimedia.3m.com/mws/media/199819O/3mtm-novectm-7200-engineered-fluid.pdf&fn=prodinfo_nvc7200.pdf (accessed December 24, 2019).

[25] D. Peng, D.B. Robinson, Ind. Eng. Chem. Fundam. 15 (1976) 59–64, doi:10.1021/i160057a011.

[26] D.S.H. Wong, S.I. Sandler, AIChE J. 38 (1992) 671–680, doi:10.1002/aic.690380505.

[27] H. Renon, J.M. Prausnitz, AIChE J. 14 (1968) 135–144, doi:10.1002/aic.690140124.

[28] Y. Peng, K.D. Goff, M.C. dos Ramos, C. McCabe, Fluid Phase Equilib. 277 (2009) 131–144, doi:10.1016/j.fluid.2008.11.008.

[29] A. Gil-Villegas, A. Galindo, P.J. Whitehead, S.J. Mills, G. Jackson, A.N. Burgess, J. Chem. Phys. 106 (1997) 4168–4186, doi:10.1063/1.473101.

[30] Y. Peng, K.D. Goff, M.C. dos Ramos, C. McCabe, Ind. Eng. Chem. Res. 49 (2010) 1378–1394, doi:10.1021/ie900795x.

[31] M.C. dos Ramos, J.D. Haley, J.R. Westwood, C. McCabe, Fluid Phase Equilib. 306 (2011) 97–111, doi:10.1016/j.fluid.2011.03.026.

[32] G.M.C. Silva, P. Morgado, J.D. Haley, V.M.T. Montoya, C. McCabe, L.F.G. Martins, E.J.M. Filipe, Fluid Phase Equilib. 425 (2016) 297–304, doi:10.1016/j.fluid.2016.06.011.

[33] S. Tamouza, J.P. Passarello, P. Tobaly, J.C. de Hemptinne, Fluid Phase Equilib. 222 (2004) 67–76, doi:10.1016/j.fluid.2004.06.038.

[34] A. Lymperiadis, C.S. Adjiman, A. Galindo, G. Jackson, J. Chem. Phys. 127 (2007) 234903, doi:10.1063/1.2813894.

[35] F.S. Emami, A. Vahid, J.R. Elliott, F. Feyzi, Ind. Eng. Chem. Res. 47 (2008) 8401–8411, doi:10.1021/ie800329r.

[36] A. Galindo, A. Gil-Villegas, P.J. Whitehead, G. Jackson, J. Phys. Chem. B 102 (1998) 7632–7639, doi:10.1021/jp9809437.

[37] C. Avendaño, T. Lafitte, C.S. Adjiman, A. Galindo, E.A. Müller, G. Jackson, J. Phys. Chem. B 117 (2013) 2717–2733, doi:10.1021/jp306442b.

[38] N. Muñoz-Rujas, F. Aguilar, J.M. García-Alonso, E.A. Montero, J. Chem. Thermodyn. 131 (2019) 630–647, doi:10.1016/j.jct.2018.12.018.

[39] G.S. Grubbs II, S.A. Cooke, Chem. Phys. Lett. 495 (2010) 182–186, doi:10.1016/j.cplett.2010.07.004.

[40] I. Bravo, Y. Díaz-de-Mera, A. Aranda, K. Smith, K.P. Shine, G. Marston, Phys. Chem. Chem. Phys. 12 (2010) 5115–5125, doi:10.1039/B923092K.

[41] M.B. Shiflett, A. Yokozeki, J. Chem. Eng. Data 52 (2007) 2413–2418, doi:10.1021/je700365z.

[42] K. Tochigi, C. Kikuchi, K. Kurihara, K. Ochi, J. Murata, K. Otake, J. Chem. Eng. Data 47 (2002) 830–834, doi:10.1021/je0102560.

[43] The Dortmund Data Bank (DDB)DDBST Software and Separation Technology, GmbH Oldenburg, Germany, 2019 Version.

[44] Y. Peng, H. Zhao, C. McCabe, Mol. Phys. 104 (2006) 571–586, doi:10.1080/00268970500475901.

[45] P.J. Leonard, D. Henderson, J.A. Barker, Trans. Faraday Soc. 66 (1970) 2439–2452, doi:10.1039/TF9706602439.

[46] M.C. dos Ramos, H. Docherty, F.J. Blas, A. Galindo, Fluid Phase Equilib. 276 (2009) 116–126, doi:10.1016/j.fluid.2008.09.025.

[47] R.L. Scott, P.H. van Konynenburg, Discuss. Faraday Soc. 49 (1970) 87–97, doi:10.1039/DF9704900087.

[48] Design Institute for Physical Property Data (U.S.) and Knovel (Firm)DIPPR Project 801, Full Version Evaluated Standard Thermophysical Property Values, BYU DIPPR, Thermophysical Properties Laboratory, Provo, Utah, 2005.

[49] S.B. Kiselev, J.F. Ely, Ind. Eng. Chem. Res. 38 (1999) 4993–5004, doi:10.1021/ie990387i.

[50] C. McCabe, S.B. Kiselev, Fluid Phase Equilib. 219 (2004) 3–9, doi:10.1016/j.fluid.2004.01.011.

[51] C. McCabe, S.B. Kiselev, Ind. Eng. Chem. Res. 43 (2004) 2839–2851, doi:10.1021/ie034288n.

[52] L. Sun, H. Zhao, S.B. Kiselev, C. McCabe, J. Phys. Chem. B 109 (2005) 9047–9058, doi:10.1021/jp044413o.